ACS OMEGA

http://pubs.acs.org/journal/acsodf

Article

Etching Kinetics of Nanodiamond Seeds in the Early Stages of CVD Diamond Growth

Raffaella Salerno, Biagio Pede, Matteo Mastellone, Valerio Serpente, Veronica Valentini, Alessandro Bellucci, Daniele M. Trucchi, Fabio Domenici, Massimo Tomellini,* and Riccardo Polini*

Cite This: *ACS Omega* 2023, 8, 25496−25505

Read Online

ACCESS | Metrics & More | Article Recommendations | Supporting Information

ABSTRACT: We present an experimental study on the etching of detonation nanodiamond (DND) seeds during typical microwave chemical vapor deposition (MWCVD) conditions leading to ultra-thin diamond film formation, which is fundamental for many technological applications. The temporal evolution of the surface density of seeds on the Si(100) substrate has been assessed by scanning electron microscopy (SEM). The resulting kinetics have been explained in the framework of a model based on the effect of the particle size, according to the Young−Laplace equation, on both chemical potential of carbon atoms in DND and activation energy of the reaction with atomic hydrogen. The model describes the experimental kinetics of seeds' disappearance by assuming that nanodiamond particles with a size smaller than a "critical radius," r^*, are etched away while those greater than r^* can grow. Finally, the model allows to estimate the rate coefficients for growth and etching from the experimental kinetics.

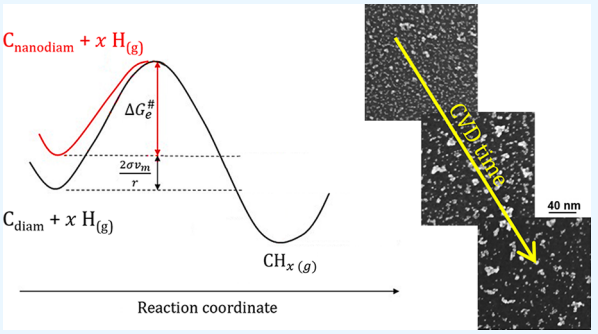

1. INTRODUCTION

Diamond is an intriguing material for applications in materials science, engineering, chemistry, and bioscience because of the unique combination of outstanding and tunable properties.[1,2] In particular, nanocrystalline diamond (NCD) is used as a functional coating in many applications[2−6] and is an emerging material for quantum information technologies[7] and advanced biolabeling.[8]

It is a well-established fact that diamond films can be grown by chemical vapor deposition (CVD) using carbon-containing gas species such as methane, aliphatic and aromatic hydrocarbons, alcohols, ketones, amines, ethers, and carbon monoxide. Methane diluted in hydrogen is the most common feed gas employed at both the laboratory and industrial scale.

Due to its large surface energy, diamond grows on heterosubstrates by the Volmer−Weber mechanism, i.e., heterogeneous nucleation and island growth at the substrate surface. However, in most CVD methods, the nucleation density of diamond islands on nondiamond surfaces is usually very low, typically in the range 10^4−10^6 nuclei/cm^2.[9,10] This implies that only rather thick (10−100 μm) closed (i.e., pinhole-free) films can be formed by impingement of the growing nuclei/islands. To get ultrathin (≤100 nm) and continuous NCD layers, nucleation densities exceeding 10^{11} cm^{-2} (10^3 μm^{-2}) are mandatory.[11−13] Therefore, several nucleation enhancement methods, including abrading with diamond grit and negative biasing of the substrate surface, have been developed to increase the nucleation densities.[14,15]

Another way to get ultrathin films is the seeding technique, i.e., the application of tiny diamond particles at the substrate surface, which act as growing centers in the subsequent CVD process.[11] The market availability of detonation nanodiamond (DND) suspensions enables the application of a large number of diamond nanoparticles per unit area, with good spatial homogeneity and size distribution. When the substrate is sonicated in a suspension of deagglomerated DNDs with the average diameter around 4−5 nm, the interaction between DNDs and the substrate surface leaves seed densities as large as 10^{12} cm^{-2}.[16] The further reduction of DNDs' average size allows to attain even larger seeds' densities (10^{13} cm^{-2}) and the growth of diamond films as thin as 5.5 nm[17,18] if proper CVD conditions are employed. S. Stehlik and coworkers wrote in a previous study:[18] "A high concentration of atomic hydrogen might also lead to a certain reduction of the nucleation density due to the possible etching of nanodiamond seeds. To suppress these effects, we performed the NCD growth at lower pressure and lower temperature." The authors had to use a linear antenna microwave (MW) plasma system ensuring both lower substrate temperature (460 °C) and lower pressure

Received: May 4, 2023
Accepted: June 16, 2023
Published: July 3, 2023

(0.11 Torr) to avoid the loss of a large majority of the extremely small (~2 nm) seeds they were able to prepare and disperse at the substrate surface. Under those specific CVD conditions, the atomic hydrogen concentration in the activated gas mixture is expected to be much lower than that typically achieved in conventional microwave (MW) CVD reactors; the deposition rate was therefore also significantly lower (≈1 nm/h). A lower deposition temperature, in combination with a low atomic hydrogen density in the plasma, was necessary for the survival of most of the 2 nm nanodiamonds during the diamond growth process. In fact, the etching of diamond in hydrogen microwave plasma is a thermally activated process, with activation energies in the interval 32−45 kcal/mol.[19,20]

Thomas et al.[21] mentioned that "After 4 min of growth ... reduction in the density of crystallites is observed." Practically, the authors noted a reduction of the initial surface density of ND seeds even if they tried to avoid the phenomenon, as they wrote in the Experimental Methods section: "During CVD, a methane fraction of 3.86% diluted in hydrogen was used to stabilize and prevent etching of the ~5 nm seeds for the first 3 min, before being reduced to 0.6% for the remainder of growth."

It is evident that DND seeds may not be stable under diamond MW CVD conditions.

In our laboratory experience, we have also noted that a fraction of DND seeds does disappear under MWCVD conditions suitable for diamond film growth. Figure 1 shows

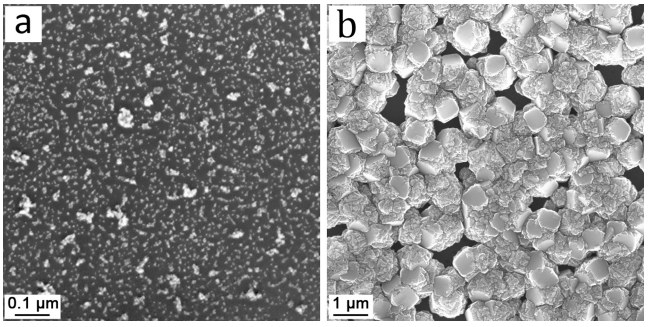

Figure 1. Si(100) substrate seeded using DND (a), 0.4 μm diamond coating deposited by MWCVD on the same seeded substrate (b). If all seeds were grown, the deposit should have been continuous.

an as-seeded Si(100) substrate (panel a, seed density > 10^{11} cm^{-2}) and the same substrate after 50 min MWCVD (840 °C, MW power = 1.25 kW, p = 40 Torr). The deposit of Figure 1b is not continuous, and its average thickness was ~0.4 μm. Considering that a seeding density exceeding 10^{11} cm^{-2} should ensure the formation of a continuous film thinner than 100 nm,[13] it follows that a fraction of the initial population of seeds did not grow.

The aim of this work is to study the kinetics of seed disappearance and to provide an explanation of this phenomenon, which, in our knowledge, has not been thoroughly investigated so far. We propose a phenomenological model for describing the behavior of the experimental kinetics of seed disappearance from the surface. The model predicts that ND etching is a particle-size dependent process, which is more effective the lower the size of the seed.

The article is divided according to the following. In Section 2, we describe the experiments of diamond growth by seeding, the characterization of the film and the procedure employed to obtain kinetic data on the etching process. In Section 3, the kinetic data are described in the framework of a kinetic model for size-dependent stability of ND. The modeling allows us to gain information on the rate coefficients for both the growth and etching process.

2. EXPERIMENTAL SECTION

2.1. Seeding and Deposition. The samples used in this work were obtained from 10 cm diameter, double-polished silicon wafers (270 ± 25 μm thickness, (100) orientation, p-type doped with boron, resistivity of 1−5 mΩ·cm, surface roughness lower than 1 nm) supplied by University Wafer Inc. The wafers were cut down to 1.5 cm × 1 cm samples that underwent a cleaning and seeding process. The cleaning composed 10 min ultrasonic bath in acetone, 10 min ultrasonic bath in 2-propanol, and 3 min ultrasonic bath in a HF:H_2O = 1:9 solution followed by an abundant rinse with deionized water. Each step was followed by drying with compressed air flow. After the cleaning steps, the samples were seeded with a detonation nanodiamond (DND) suspension obtained by mixing commercially available DND suspension in dimethyl sulfoxide (*Blueseeds*, by Adámas Nanotechnology, 0.5% w/v ND in DMSO) and methanol in 1:3 ratio.[22] The substrates were immersed in the DND suspension and sonicated for 15 min in ultrasonic bath. Finally, the substrates were rinsed with methanol and dried under compressed air flow. An average seeding density of (7 ± 2) × 10^{11} cm^{-2} was obtained after the process (Figure 2, top panel). In order to determine the DND particle density before and after each CVD process, the seeded substrates were delicately cleaved: one-third of the substrate was set aside in order to measure the surface density of seeds by SEM; the remaining 1 cm × 1 cm sample was loaded into the CVD chamber.

Diamond growth was accomplished via a customized microwave-plasma assisted CVD ASTeX reactor equipped with an MKS Instruments TM025 51 microwave generator operating at 2.45 GHz frequency. After placing the substrate on top of a molybdenum disc positioned on the graphite stage in the reaction chamber, the pressure was lowered to 2 × 10^{-6} Torr at which point the temperature was gradually raised to 700 °C while keeping the pressure below 9 × 10^{-6} Torr (substrate temperature was controlled with a thermocouple positioned inside the graphite stage). Once the base pressure returned to 2 × 10^{-6} Torr, hydrogen and methane were introduced in the reaction chamber. The methane concentration was either 0.5 or 1 vol %. The total gas flow was 200 standard cubic centimeter per minute (sccm). Microwave power used in this work was 300, 600, or 800 W; to guarantee a stable plasma discharge in the MW CVD reactor, we used 8, 24.5, and 27 Torr deposition pressure, respectively. The deposition time was counted starting when the plasma was ignited and ended when the plasma was shut down. The surface temperature of the substrate was checked to be within 700 ± 10 °C with a two-color IR pyrometer during the deposition time. After shutting down the plasma, the methane flow was cut off and the temperature was gradually lowered back to room temperature.

2.2. Characterization. The DND particle size distribution in the suspension employed for substrate seeding was assessed by photon correlation spectroscopy (PCS) using a Malvern Instrument Zetasizer Nano ZS equipped with a 4 mW helium−neon laser (632.8 nm); the scattering angle was 173°. A refractive index of 1.352 and a viscosity equal to 0.722 mPa·s at

https://doi.org/10.1021/acsomega.3c03080
ACS Omega 2023, 8, 25496−25505

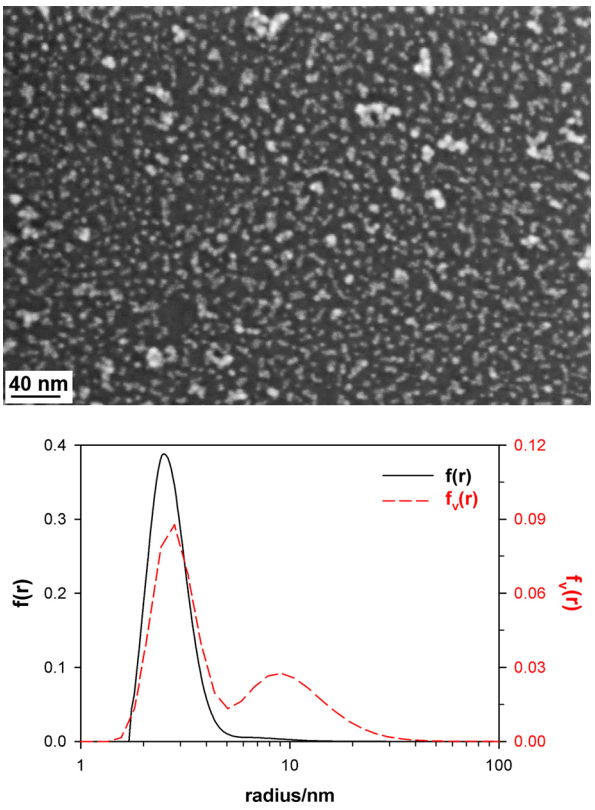

Figure 2. SEM micrograph of DNDs seeded on the Si(100) substrate by treating it in an ultrasonic bath with 1 part of 0.5% w/v DND in DMSO and 3 parts of CH_3OH. The plot shows the size distribution by volume, $f_v(r)$, (red dotted line), and the size distribution by number, $f(r)$ (black line), of the suspension used for the seeding. The $f_v(r)$ was obtained by PCS; the $f(r)$ was calculated from the $f_v(r)$.

20 °C of the DND dispersion medium (1 part DMSO and 3 parts methanol) were used to convert the measured intensity/size distribution to volume/size distribution ($f_v(r)$; see Figure 2, bottom panel).

Field emission gun scanning electron microscopy (FEG SEM, Zeiss LEO Supra 35) was used to determine seeding density, as well as surface morphology and thickness of the deposited NCD films. All SEM images were acquired at 10 kV in the regime of secondary electrons (SEs), using the Inlens SE detector of the microscope. SEM micrographs were analyzed by ImageJ software to estimate the surface density of diamond seeds/crystallites. It is worth recalling that growing diamond particles do not coalesce; they impinge, i.e., no redistribution of matter occurs after collision among islands. On impingement, grain boundaries between diamond crystallites form. Consequently, image analysis was performed by considering grain boundaries detected in SEM pictures, i.e., by counting impinging grains as separate entities. The same criterion has been used for particle counting in DND agglomerates at the surface of as-seeded substrates.

Raman spectroscopy measurements were carried out using a Horiba Scientific LabRam HR Evolution confocal spectrometer equipped with a 100 mW laser source (wavelength of 532 nm, by Oxxius SA, France); a computerized *XY*-table, an electron-multiplier CCD detector, an Olympus U5RE2 microscope with 100× objective (laser spot on the sample surface 0.7 μm) with a numerical aperture (NA) of 0.9, and a grating with 600 grooves/mm were used. All Raman spectra were recorded in backscattering geometry focalizing 100 mW at the sample surface; twenty spectra with an accumulation time of 10 s were averaged.

Numerical computations have been performed using the Wolfram Mathematica package.

3. RESULTS AND DISCUSSION

3.1. Size Distribution of the DND Suspension. Figure 2 illustrates the results of DND seeding with a small average aggregate size.

The $f_v(r)$ distribution function (red dotted line) was bimodal, with two modes at 2.8 and 9 nm of radius. The second peak in the probability density function accounts for 34% of total volume. These findings are in excellent agreement with previous results published by Shenderova et al., who used the same suspension (Figure 3 of ref 22[2]). The $f(r)$ distribution function (black line in Figure 2), i.e., the fraction of particles ($f(r)dr$) with radius in the range (r, $r + dr$) at r, was derived from the $f_v(r)$, as detailed in the Supporting Information. The second mode of the $f_v(r)$ is not clearly visible anymore in the size distribution function, $f(r)$.

3.2. Stability of DND Seeds under High Vacuum Annealing and H_2 Plasma Exposure. As pointed out in the Introduction, preliminary results had provided indirect evidence that a fraction of initial seeds was missing after CVD (see Figure 1). The seeds could have disappeared during

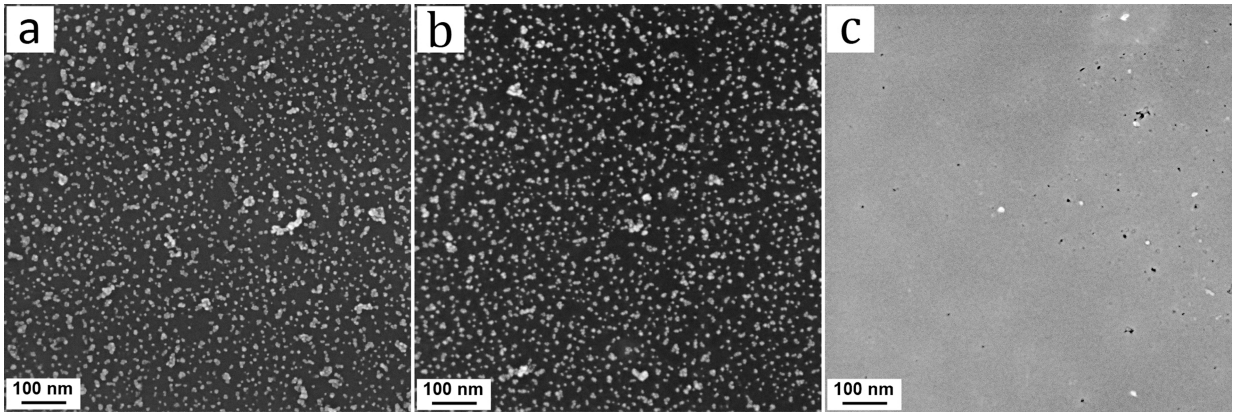

Figure 3. SEM micrographs of DNDs seeded on the Si(100) substrate (a), after 48 h annealing at 700 °C in high vacuum (b) and after 10 min H_2 plasma exposure at 700 °C, 600 W, 24 Torr (c).

https://doi.org/10.1021/acsomega.3c03080
ACS Omega 2023, 8, 25496−25505

Table 1. DND Seeds' Evolution after Short MWCVD Deposition Runs[a]

MW plasma power (W)	CH_4%	p (Torr)	CVD duration (t, min)	$N(0)/cm^{-2}$	$N(t)/cm^{-2}$	N %
300	0.5	8	3	$(7.9 \pm 0.4) \times 10^{11}$	$(5.3 \pm 0.4) \times 10^{11}$	67 ± 6
			5	$(8.0 \pm 0.4) \times 10^{11}$	$(4.8 \pm 0.3) \times 10^{11}$	60 ± 5
			10	$(7.2 \pm 0.5) \times 10^{11}$	$(3.7 \pm 0.3) \times 10^{11}$	51 ± 5
			40	$(10.6 \pm 0.2) \times 10^{11}$	$(1.6 \pm 0.2) \times 10^{11}$	15 ± 2
600	0.5	24.5	3	$(8.2 \pm 0.1) \times 10^{11}$	$(5.3 \pm 0.2) \times 10^{11}$	65 ± 2
			5	$(6.3 \pm 0.2) \times 10^{11}$	$(3.5 \pm 0.1) \times 10^{11}$	56 ± 2
			10	$(7.7 \pm 0.6) \times 10^{11}$	$(3.1 \pm 0.2) \times 10^{11}$	40 ± 4
600	1	24.5	2	$(8.0 \pm 0.3) \times 10^{11}$	$(5.5 \pm 0.2) \times 10^{11}$	69 ± 4
			3	$(5.5 \pm 0.1) \times 10^{11}$	$(3.6 \pm 0.1) \times 10^{11}$	65 ± 2
			5	$(6.3 \pm 0.2) \times 10^{11}$	$(3.5 \pm 0.1) \times 10^{11}$	56 ± 2
			7	$(7.8 \pm 0.1) \times 10^{11}$	$(2.5 \pm 0.2) \times 10^{11}$	32 ± 3
800	0.5	27	2	$(9.0 \pm 0.3) \times 10^{11}$	$(6.3 \pm 0.1) \times 10^{11}$	70 ± 3
			3	$(6.9 \pm 0.3) \times 10^{11}$	$(4.2 \pm 0.1) \times 10^{11}$	61 ± 3
			5	$(8.9 \pm 0.2) \times 10^{11}$	$(4.8 \pm 0.3) \times 10^{11}$	54 ± 4

[a]Substrate temperature was 700 °C.

diamond CVD for two reasons: (a) etching/gasification performed by the activated gas phase, (b) high-temperature solid-state reaction between sp^3 carbon and silicon substrate. To check if ND seeds were thermally stable at the deposition temperature, we subjected as-seeded Si(100) to prolonged annealing (48 h at 700 °C) in the MW CVD reactor under high vacuum ($p = 2 \times 10^{-7}$ Torr). Figure 3 displays the SEM micrographs of the as-seeded substrate (panel a) and of the same sample after annealing (panel b). The seed density did not change, thus indicating that DND particles deposited at the Si(100) surface are stable at 700 °C. These findings confirm previously published results.[23]

We also checked the stability of DND seeds under H_2 plasma exposure in our MWCVD reactor, without methane in the feed gas. Panel c of Figure 3 displays the Si(100) substrate surface after 10 min of H_2 exposure at 700 °C and 600 W microwave power (p = 24 Torr).

It is evident that almost all of the seeds have disappeared, with just few particles left at the Si(100) surface. The bright particles visible in Figure 3, panel c, represent what remained of the largest agglomerates initially present. If we consider that most of the seeds (≥99.9%) were etched away, we have calculated, as discussed in Section 3.4, that the rate of etching under pure H_2 plasma exposure was at least 0.4 nm/min (≥24 nm/h). J.C. Arnault and coworkers[24] estimated a nanodiamond etching rate lower than 4.4 nm/h under H_2 plasma at even a higher temperature (T = 940 °C). The nearly one order of magnitude larger etching rate we have observed at 700 °C might be ascribed to a larger plasma density and/or to a higher atomic hydrogen concentration at the substrate surface in our reactor.

Atomic hydrogen not only eliminated the DND particles but caused the etching of Si(100), resulting in the formation of the dark etch pits detected by SEM (Figure 3c).[25]

Therefore, our preliminary seed stability scouting investigation demonstrated that (i) DND seeds on Si(100) are thermally stable at the CVD temperature we employed for studying seeds' density evolution under diamond CVD conditions and (ii) DND seeds are quickly gasified when exposed to pure H_2 plasma in our MWCVD reactor.

3.3. Stability of DND Seeds under Diamond MWCVD.

The aim of this work was to study the (in)stability of DND particles acting as growth centers in the deposition of NCD films. We performed short deposition runs to study the time evolution of DND seeds at the substrate surface, by selecting different deposition conditions that allow the formation of diamond films.

Table 1 summarizes the depositions we performed leading to noncontinuous deposits. $N(0)$ represents the initial seed density for a given sample, $N(t)$ is the density of crystallites after t min CVD, N % = 100 × $N(t)/N(0)$ is the percentage of crystallites remaining on the substrate surface after t min CVD. For each sample, we used five SEM micrographs to determine $N(0)$ and $N(t)$ by image analysis.

With the only exception of data at 300 W (0.5% CH_4), it was not possible to get meaningful $N(t)$ values for CVD times longer than 10 min, due to the quick coverage of the substrate surface caused by growing seeds.

Figure 4 shows the SEM micrographs of samples subjected to 3- and 5-min CVD. It is worth comparing those micrographs to the SEM image in Figure 2, showing the larger DND surface density (N % = 100) of a typical as-seeded substrate.

In Table 2, the CVD durations at film closure, i.e., when substrate coverage approaches 100%, are reported, as well as thickness and deposition rate of the continuous films. The morphology and Raman spectra of these films are displayed in Figures S1 and S2 of the Supporting Information, respectively.

The data show that, by using 600 and 800 W microwave (MW) power, the surface density of initial seeds decreased (see Table 1) while some seeds did actually grow (Figure 4). A different scenario occurred at 300 W, where a significant crystallite growth did not occur even after 40 min, although the surface density of seeds continued to decrease with CVD time (see Figure S3).

To check if diamond could grow by using such a low plasma power, we put in the CVD chamber the sample previously coated with 52 nm continuous film deposited for 15 min at 800 W, 0.5% CH_4 (Table 2). This sample was subjected to a second CVD run for 300 min CVD, at 300 W, 0.5% CH_4. The thickness of the previously prepared NCD film augmented from 52 to 180 nm. This experimental result indicates that when a continuous NCD film was exposed to the same MWCVD conditions that caused seeds disappearance, its thickness did increase, with a rate, in this specific case, of 0.43 nm/min: the growth rate of "flat" diamond is larger than that of the seeds. Similar results were reported by A. Giussani and coworkers;[26] these authors used a O_2 containing feed gas in the MWCVD reactor (1% CH_4, 1% O_2, 98% H_2, Si(100) substrate,

https://doi.org/10.1021/acsomega.3c03080
ACS Omega 2023, 8, 25496−25505

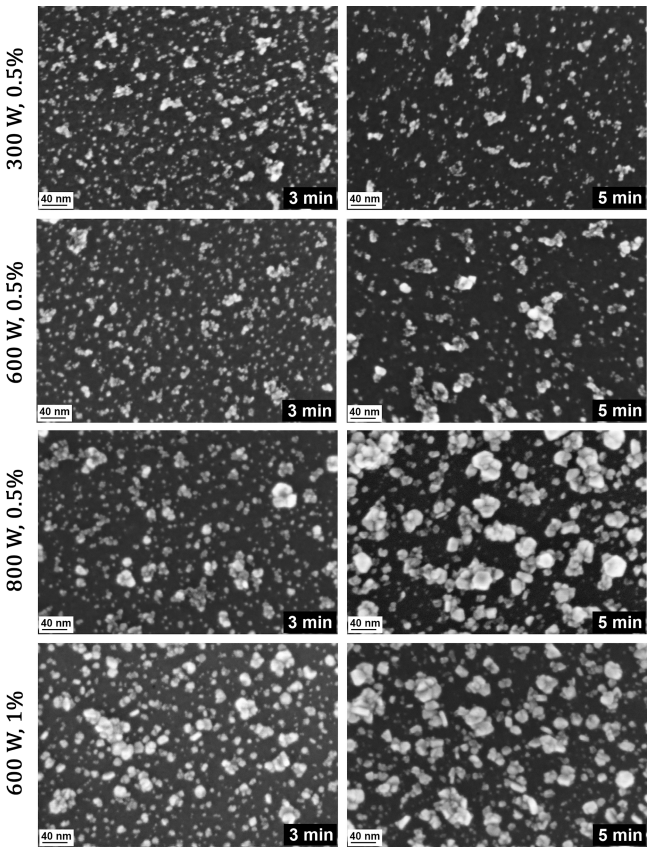

Figure 4. SEM micrographs of nanodiamond crystallites after 3- and 5-min deposition runs (see Table 1 for surface densities).

Table 2. Thickness of the Continuous NCD Films at Closure and Corresponding Deposition Conditions and Growth Rates

MW plasma power (W)	CH_4%	p (Torr)	time at film closure (t, min)	film thickness (nm)	deposition rate (nm/min)
300	0.5	8			
600	0.5	24.5	20	39 ± 4	1.9 ± 0.2
600	1	24.5	12	45 ± 11	3.7 ± 0.9
800	0.5	27	15	52 ± 10	3.5 ± 0.7

T = 798 ± 7 °C): by employing the same MWCVD conditions which caused all seeds to disappear on Si(100), they could increase the thickness of a diamond film previously prepared.

Consequently, considering that DND seeds on Si(100) are thermally stable at 700 °C, the decrease of the surface density of nanodiamonds must be ascribed to the etching of some seeds, while some other seeds can survive and/or act as growth centers till the closure of the film. A spontaneous question arises at this point: which seeds are disappearing and why?

3.4. Kinetic Approach for the Size-Dependent Stability of DND. In this section, we present a kinetic model for the etching of ND particles, by taking into account the effect of the seed size on kinetics. The etching mechanism of diamond includes numerous surface chemical reactions, but, as is shown in a previous study,[27] only few of them play a principal role in the process. Therefore, we consider here the following schematic reaction for the etching of nanodiamond:

$$C_{(s)} + x\ H_{(g)} \rightarrow CH_{x\ (g)} \quad (1)$$

where $C_{(s)}$ stands for sp^3 carbon atoms in the ND, eventually bonded to adsorbed hydrogen atoms,[3] and $H_{(g)}$ is atomic hydrogen in the plasma. Seeds can be grouped in dependence of their volume, say v_0, from which an equivalent radius, r_0, is defined: $r_0 = \left(\frac{3}{4\pi}v_0\right)^{1/3}$. We stress that, owing to the detonation production process of DND, seeds with the same size could have, in general, different shapes, or crystal habits.[28] Since the etching rate is expected to depend upon the habit, in the following, the etching rate of the set of seeds with size r_0 is to be intended in the statistical sense, i.e., as an average quantity. Details on the approximations employed in order to formulate the model in the closed form are reported in the Supporting Information (Section III).

The rate of the etching reaction (moles/s) is a function of temperature and gas phase composition (that is considered to be time-independent) according to $\left(\frac{dn}{dt}\right)_e = K'_e(T, r)\cdot s/v_m$ where v_m is the molar volume, $s = 4\pi r^2$ is the surface of the seed particle, assumed spherical, r is the radius, and K'_e is the rate coefficient of the forward reaction 1. In particular, $K'_e(T, r) = \nu e^{-\Delta G^{\#}_e(r, T)/RT}$ with ν as the pre-exponential factor and $\Delta G^{\#}_e(r, T)$ as the activation free energy depending on gas phase composition and seed size. This last dependence is ascribed to the size dependence of the chemical potential of the solid reactant, namely, the sp^3 C atoms, that is related to the surface tension of the crystal. The increment of the chemical potential of C in the ND particles is due to the increase of stress as given by the Young−Laplace equation. This contribution does reduce the energy barrier according to $\Delta G^{\#}_e(r, T) = \Delta g^{\#}(T) - \frac{2\sigma v_m}{r}$, where σ is the surface tension of diamond, v_m is the molar volume, and $\Delta g^{\#}(T)$ is the activation energy in the absence of the Young−Laplace (YL) term. It is worth noting that the YL equation plays a key role in describing the thermodynamics of systems at the nanoscale.[29] In addition, the YL equation has been used to extrapolate the diamond−graphite P−T equilibrium phase diagram to the nanometer-scale region.[30]

Alternatively, we can attain a similar result by exploiting the detailed balancing for the reaction above, according to $\frac{K_e^{(f)}}{K_e^{(b)}} = e^{-\Delta G^0/RT}$ with $K_e^{(b)}$ and $K_e^{(f)}$ rate constants of the backward and forward reactions, respectively, and ΔG^0 the standard free energy change of reaction 1. It stems that $(\Delta G^0(r) - \Delta G^0(\infty)) = -\frac{2\sigma v_m}{r}$ that leads to $K_e^{(f)}(r) = K_e^{(f)}(\infty)e^{2\sigma v_m/rRT} = \nu e^{\Delta g^{\#(0)}(T)/RT}e^{2\sigma v_m/rRT}$, where the rate constant of the reverse reaction has been considered independent of r.

On the other hand, the growth reaction is also proportional to the particle surface area (i.e., to the number of adsorption site[31]) as $\left(\frac{dn}{dt}\right)_g = K_g(T)\cdot s/v_m$ where $K_g(T) = \nu e^{-\Delta G^{\#}(T)/RT}$, with size-independent activation energy. A pictorial view of the effect of the particle size on the energy barrier is displayed in Figure 5.

In the figure, we also indicate the reaction affinity, i.e., $A = \sum_i \nu_i \mu_i$, with ν_i stoichiometric coefficients (positive and negative for products and reactants, respectively) and μ_i chemical potentials. Specifically, the chemical potentials are

https://doi.org/10.1021/acsomega.3c03080
ACS Omega 2023, 8, 25496−25505

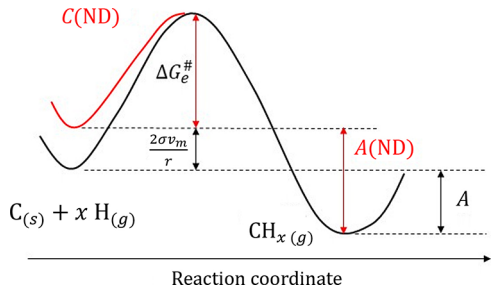

Figure 5. Pictorial view of the free energy profile for the etching reaction of C in nanodiamond particles. The free energy curves, with and without the inclusion of the size effect, are displayed as red and black lines, respectively. In the figure, A is the affinity of the etching reaction, that is, a decreasing function of the radius of the ND particle. The increase of the free energy of the reactants for the ND etching reaction is due to the increase of the chemical potential of C in nanometric crystals, when compared to that in the limit of infinite crystal ($r \to \infty$).

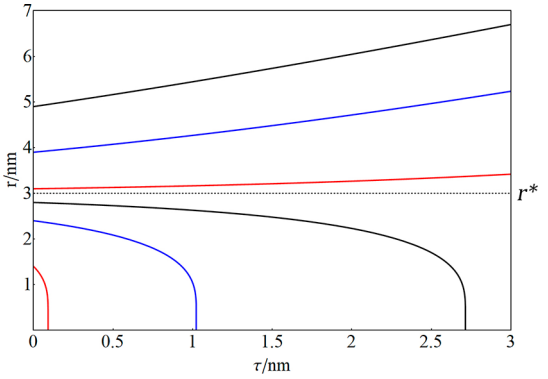

Figure 6. Numerical solution of the kinetics of growth and shrinkage for ND seeds having $r_0 > r^*$ and $r_0 < r^*$, respectively. Computations have been done for $r^* = 3$ nm and $c = 3.06$ nm. τ is the reduced time and has a dimension of a length (see text).

$\mu_C(r) = \mu_C(\infty) + \frac{2\sigma v_m}{r}$, $\mu_H = \mu_H^0 + RT \ln P_H/P^0$ and $\mu_{CH_x} = \mu_{CH_x}^0 + RT \ln P_{CH_x}/P^0$.

The net rate of growth is therefore given by $\left(\frac{dn}{dt}\right) = \{-K_e'(T, r)\cdot s + K_g(T)\cdot s\}/v_m$, that is, ($n = \frac{4\pi r^3}{3v_m}$, $s = 4\pi r^2$):

$$\frac{dr}{dt} = -K_e e^{c/r} + K_g \tag{2}$$

where $K_e = \nu e^{-\Delta g^{\#}(T)/RT}$ and $c = 2\sigma v_m/RT$. Integration of eq 2 provides the $r(r_0, t)$ function that is here intended as the evolution of the average radius of the r_0-population of seeds. In other words, as anticipated above, owing to the polydispersivity of diamond nanoparticles and the dependence of the rate of etching on crystal face, r and K_e are considered average quantities. The generalization of eq 2 to the case of an anisotropic *faceted-crystal* is discussed in the Supporting Information (Section III).

By denoting with $k_g = K_g - K_e$ the net rate of ND growth in the absence of the YL term, the rate equation eq 2 can be rewritten in the form

$$\frac{dr}{d\tau} = \frac{k_g}{|k_g|}\frac{\exp(c/r^*) - \exp(c/r)}{\exp(c/r^*) - 1} \tag{3}$$

where $\tau = t|k_g|$ is the reduced time (dimension of a length), and the parameter $r^* = \frac{c}{\ln(K_g/K_e)} = \frac{c}{\ln(1 + k_g/K_e)}$ has been defined. In eq 3, r^* is positive-definite for $k_g > 0$, namely, $K_g > K_e$. On the other hand, for $k_g < 0$, i.e., $K_g < K_e$, r^* is negative-definite and $\frac{dr}{d\tau}$ is lower than zero for any value of the seed size; in this latter case, all ND particles undergo an etching process and are removed from the substrate.

Eq 3 shows that, for $r_0 < r^*$, ND particles shrink and are then etched away completely from the substrate. The opposite occurs for larger seeds ($r_0 > r^*$) where the growth prevails. A set of typical solutions of eq 3 for initial sizes of seeds larger and smaller than r^* are reported in Figure 6. According to eq 3, the seeds with the initial radius close to r^* will grow at a very low rate.

It is worth noting that a slightly different approach, based on the *kinetic law of mass action*,[32,33] actually leads to an equation similar to eq 2.

In the following, we briefly summarize the method employed for modeling the time dependence of the number density of seeds, $N(t)$, during the CVD treatment.

For given r^* and c, the numerical integration of eq 3 allows one to compute the time dependence of the mean size of the seed population with initial size r_0: $r = r(r_0, \tau)$. For a positive value of r^* and $r_0 < r^*$, the mean radius vanishes at a certain time, say $\tau = \tau_s$, that implies $r(r_0, \tau_s) = 0$. In this last equation, τ_s has the meaning of mean-lifetime of the seeds with initial size r_0. The explicit form of this relation in the end provides the function $\tau_s = \tau_s(r_0)$.

Based on the statistical significance of τ_s, it is possible to include statistical fluctuations of crystal habit into the kinetic model. For a given set of seeds with mean-lifetime $\tau_s(r_0)$, Poisson statistic provides $\frac{dn}{d\tau} = -\frac{n}{\tau_s(r_0)}$, where n is the surface density of the considered set of the r_0-ensemble of seeds. Integration of the equation yields

$$n(r_0, \tau) = n(r_0, 0)e^{-\tau/\tau_s(r_0)} \tag{4}$$

where $n(r_0,0)$ is the initial density of seeds ($\tau = 0$).

To determine the kinetics of the number density of seeds, we resort to the probability density function (PDF) of the deposited ND, $f(r_0)$. As anticipated, the experimental PDF is well described by a log-normal distribution. Specifically, the experimental PDF, as a function of particle radius, is given by the log-normal with mean and variance equal to $m = 0.996$ and $v = 0.22$, respectively, as obtained by the fitting procedure. At reduced time τ, the number of seeds belonging to the r_0-population, still present on the surface, is given by eq 4 in terms of $f(r_0)$ according to

$$dn(r_0, \tau) = N(0)e^{-\tau/\tau_s(r_0)}f(r_0)dr_0 \tag{5}$$

where $N(0)$ is the initial surface density of seeds. The kinetics of the number of etched seeds is given by integrating eq 5: $N_e(\tau) = \int_0^{r^*} dn(r_0, \tau)$ while the number of growing seeds, with $r > r^*$, equals $N_g(\tau) = N(0)\int_{r^*}^{\infty} f(x)dx$. The total number of seeds as a function of reduced time is therefore given by $N(\tau) = N_g(\tau) + N_e(\tau)$, namely,

https://doi.org/10.1021/acsomega.3c03080
ACS Omega 2023, 8, 25496−25505

$$\frac{N(\tau)}{N(0)} = 1 - \int_0^{r^*} f(x)\mathrm{d}x + \int_0^{r^*} \mathrm{e}^{-\tau/\tau_s(x)} f(x)\mathrm{d}x$$
$$= 1 - \int_0^{r^*} f(x)(1 - \mathrm{e}^{-\tau/\tau_s(x)})\mathrm{d}x \quad (6)$$

The value of the cut off radius, r^*, can be estimated from the experimental $\frac{N(t)}{N(0)}$ curve at a longer time, say τ^*, when $N(t)$ reaches a stationary value. This figure is representative of the total number of seeds surviving on the surface, which contribute to the film growth. By denoting with $\theta = \frac{N(\tau^*)}{N(0)}$, the steady-state value of seeds, eq 6 provides $\theta = \int_{r^*}^{\infty} f(x)\mathrm{d}x$ from which r^* can be estimated. The knowledge of r^* allows us to integrate eq 3 and to determine the $\tau_s(r_0)$ function which enters eq 6.

In Figure 7, the results of the modeling are compared to the experimental data points (Table 1) for several deposition conditions.

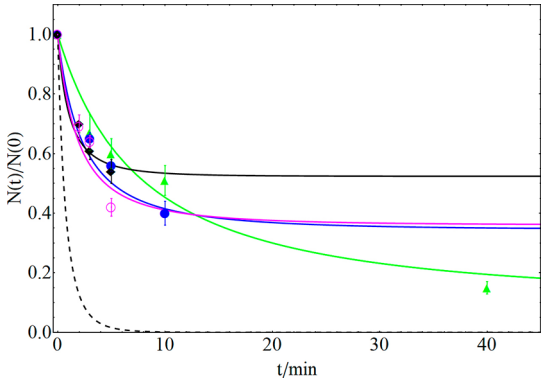

Figure 7. Comparison between the experimental kinetics of seed disappearance ($N(t)/N(0) = N$ % /100, see Table 1, does represent the fraction of initial seeds at time t) and the model. Parameter values employed in the numerical integration of eq 2 are c = 3.06 nm and r^* = 3.58 for 300 W and 0.5% CH_4 (green triangles), r^* = 2.95 for 600 W and 0.5% CH_4 (blue full circles), r^*= 2.67 for 800 W and 0.5% CH_4 (black full diamond), and r^*= 2.92 nm for 600 W with 1% CH_4 (magenta open circles). The mean values of the growth rates are 300 W, 0.5% CH_4, k_g = 0.09 nm min^{-1}; 600 W, 0.5% CH_4, k_g = 0.4 nm min^{-1}; 800 W, 0.5% CH_4, k_g = 0.95 nm min^{-1}; 600 W, 1% CH_4, k_g = 0.5 nm min^{-1}. Dashed line is the kinetics of etching in pure H_2 plasma estimated from Figure 3c (see text for details).

In the model, a constant value of c, and therefore of σ, has been taken for all the curves, while k_g was the only fitting parameter. Specifically, to estimate the c parameter, a mean value of diamond surface tension was employed, according to a previous report.[34,44] The k_g parameter is found to increase with the microwave plasma power, in agreement with the experimental evidence according to which the higher the power, the larger the growth rate of the film. However, it is important to remember that k_g is for the growth of the ND and can be different from that of a continuous thin film. In fact, the growth rate of thicker microcrystalline diamond (MCD) films was found to be greater than that of ultrathin NCD films (see the Supporting Information, Table S1 and Figure S6).

In Figure 8, we report the behavior of the density of seeds that survived the etching process as a function of the ratio $\frac{k_g}{K_e} > 0$. The computation is performed through the expression

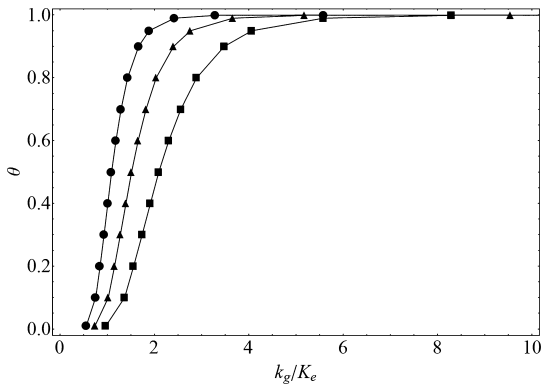

Figure 8. Fraction, θ, of the seed population that contributes to the film growth as a function of the $(K_g - K_e)/K_e = k_g/K_e$ ratio. Computations were performed using the $f(r)$ derived from PCS data (see Figure 2) and for c = 2 nm (solid circle), c = 2.5 nm (solid triangle), and c = 3.06 nm (solid square).

$\theta\left(\frac{k_g}{K_e}\right) = \int_{c/\ln(K_g/K_e)}^{\infty} f(x)\mathrm{d}x$, using the lognormal distribution, $f(r)$, displayed in Figure 2 and derived from PCS data.

From Figure 8 (c = 3.06 nm curve) and the k_g values obtained from the kinetic data (Figure 7), we computed the K_e and K_g values reported in Figure 9A. In fact, from the knowledge of the experimental density of seeds left on the surface (θ) and the plot of Figure 9A, it is possible to estimate the ratio of these rate coefficients. Besides, since $k_g = K_g - K_e$, the values of both these quantities can be finally obtained. In the figure, solid and open symbols refer to diamond deposition with 0.5 and 1% CH_4 in the feed gas, respectively. The net rates of growth of ND derived by the present model, k_g, are displayed in panel B of Figure 9 (squares). In the same plot, the growth rates of the film at closure (Table 2) are also displayed as triangles; full symbols refer to 0.5% CH_4 and open symbols refer to 1% CH_4. The difference between the growth rates of seeds and NCD films at closure is attributable to the change of the crystalline habit of the seeds upon etching, where some crystal faces could be preferentially etched. Under this assumption, the crystal habits with higher k_g are thought to be "selected" by the etching process; this implies an increase of the k_g values as deposition proceeds. As far as the data at 600 W are concerned, the rate coefficients for etching, K_e, for 0.5 and 1% CH_4 are 0.27 and 0.33 nm min^{-1}, respectively. We point out that, different from the K_g quantities, these etching rate constants are very similar. Besides, these K_e values are lower than that estimated for etching in pure hydrogen plasma (600 W) and equal to 0.4 nm/min. This rate has been computed through the present modeling at K_g = 0, by assuming that 99.9% of initial seeds were missing after 10 min H_2 plasma exposure (Figure 3c). The corresponding etching kinetics is displayed in Figure 7 as dashed lines. We recall that the etching rate constant the model predicts in the absence of methane in the feed gas is a rough underestimate we attempted by using one experiment only (Figure 3c). Anyway, its larger value compared to the K_e constants at 600 W of Figure 9A is reasonable and attributable to a higher atomic hydrogen concentration in pure H_2 plasma discharge in that H atoms can be consumed in the reaction $CH_4 + H \rightarrow CH_3 + H_2$.[31,35]

Before concluding this section, we stress that under similar experimental conditions (800 W, 0.5% CH_4, p = 27 Torr, t = 120 min), heterogeneous nucleation took place on the Si(100)

https://doi.org/10.1021/acsomega.3c03080
ACS Omega 2023, 8, 25496−25505

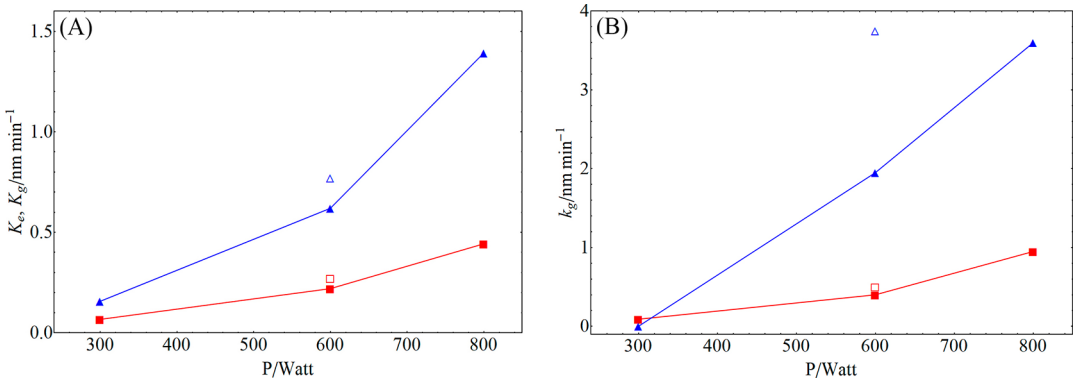

Figure 9. Panel (A): Behavior of the rate coefficients for growth (K_g, triangles) and etching (K_e, squares) as a function of microwave power, P, in the plasma. Solid symbols refer to deposition experiments carried out with 0.5% CH_4; open symbols refer to the deposition experiment with 1% CH_4 (600 W). Panel (B): Comparison between the net rate of growth (k_g) of a diamond film at closure (triangles) and the ND particles as derived by the kinetic model. Like in panel (A), solid and open symbols refer to depositions with 0.5% CH_4 and 1% CH_4, respectively.

substrate without any seeding pretreatment. As expected, we measured a nucleation density lower than 10^6 cm^{-2}, i.e., more than five orders of magnitude less than seeding density (Figure S5). The question therefore arises on how to reconcile the size-dependent etching above discussed with the heterogeneous nucleation. In fact, heterogeneous nucleation implies the formation of critical clusters with radius surely lower than the r^* value we found as a threshold limit for the stability of DND seeds in our experiments ($r^* \cong 3$ nm, corresponding to 2×10^4 carbon atoms). This aspect can be tackled by considering, in the kinetic model, the effect of the interaction between the substrate and diamond. For this system, the chemical potential of C in ND is estimated on the basis of the Gibbs model of interface. The computation provides the expression (see Section V of the Supporting Information for details):

$$\mu_C = \mu_C(\infty) + \left(\frac{3}{2} - \frac{\beta}{2\sigma}\right)\frac{2\sigma v_m}{r} \quad (7)$$

where β is the work of adhesion. An estimate of the radius-dependent term in eq 7 can be obtained through the Born–Stern approach.[36] By setting $\beta \cong \varepsilon_{Si-C}$ and $2\sigma \cong \varepsilon_{C-C}$, ε being the bonding energies between the stated couple of atoms in diamond (3.673 eV, ref 37) and SiC (4.6 eV, ref 38), we get $\left(\frac{3}{2} - \frac{\varepsilon_{Si-C}}{\varepsilon_{C-C}}\right) \cong 0.25$. A similar figure is attained by employing the work of adhesion, $\beta = 9.15$ J/m^2, recently calculated for diamond (001)–Si(001), as shown in a previous study.[39] In this case, we get $\left(\frac{3}{2} - \frac{\beta}{2\sigma_{cv}}\right) = 0.23$. The above computations imply a reduction of the c term entering eq 2, with a parallel decrease of the r^* value down to 0.69–0.75 nm[5] (r^* was around 3 nm for seeds). It is worth mentioning that the size of the critical nucleus in diamond heterogeneous nucleation is still a debated topic. S.T. Lee and coworkers hypothesized that the critical size of the nucleus should be less than 2 nm ($r < 1$ nm), which was the size of the smallest diamond crystallite on silicon they could detect by high-resolution transmission electron microscopy (HRTEM).[40] Other authors have estimated critical nuclei of a few tens of atoms.[41,42] The aim of this work is not to determine the critical size of the diamond nucleus but rather to provide a rationale for what experimentalists have been observing since years. Eq 7 suggests that crystallites nucleated from the gas phase, and smaller than DND particles, may be stable toward etching under CVD conditions, thanks to the stronger interaction with the substrate.

4. CONCLUSIONS

For the first time, a physical model to explain the DND seeds' gasification by atomic hydrogen under typical diamond CVD conditions has been proposed. This phenomenon has been depicted by introducing a size-dependent activation energy for the etching reaction. In the model, the stress due to particle curvature, according to the Young–Laplace equation, does increase the chemical potential of carbon atoms in DND, thus reducing the activation energy of the etching reaction. The approach predicts that seeds with a radius lower than a critical value, r^*, do not survive the CVD process. The r^* quantity depends on (i) the ratio of rate coefficients for growth (K_g) and etching (K_e), (ii) surface tension of diamond, and (iii) deposition temperature. Under our experimental conditions, r^* varied between 2.7 and 3.6 nm and increased with microwave power when methane concentration and substrate temperature were kept constant. For a given size distribution function of seeds having minimum size smaller than r^*, the lower the r^* value, the larger the fraction of seeds that will survive and grow.

Finally, it is worth pointing out that the present approach provides an indirect proof of the dependence of the net rate of growth on the seed size through modeling of experimental kinetic data, $N(t)$. The measurements, e.g., by AFM, of ND particle size distribution functions before and after CVD could further validate the hypothesis that the etching rate of seeds by atomic hydrogen is size-dependent under CVD growth conditions. An important improvement of this research topic should certainly arise from the observation of individual crystals before and after few minutes of CVD.

■ ASSOCIATED CONTENT

Supporting Information

The Supporting Information is available free of charge at https://pubs.acs.org/doi/10.1021/acsomega.3c03080.

Derivation of $f(r)$ from $f_v(r)$; additional SEM pictures and Raman spectra; molar free energy of a faceted crystal; growth rates of NCD films at coalescence and of MCD films; and the case of heterogeneous nucleation (PDF)

https://doi.org/10.1021/acsomega.3c03080
ACS Omega 2023, 8, 25496–25505

AUTHOR INFORMATION

Corresponding Authors

Massimo Tomellini − *Dipartimento di Scienze e Tecnologie Chimiche, Università di Roma "Tor Vergata" and Consorzio INSTM RU "Roma Tor Vergata", Rome 00133, Italy*; Email: tomellini@uniroma2.it

Riccardo Polini − *Dipartimento di Scienze e Tecnologie Chimiche, Università di Roma "Tor Vergata" and Consorzio INSTM RU "Roma Tor Vergata", Rome 00133, Italy*; orcid.org/0000-0002-6551-0883; Email: polini@uniroma2.it

Authors

Raffaella Salerno − *Dipartimento di Scienze e Tecnologie Chimiche, Università di Roma "Tor Vergata" and Consorzio INSTM RU "Roma Tor Vergata", Rome 00133, Italy; Istituto di Struttura della Materia (ISM), Consiglio Nazionale delle Ricerche (CNR), Sez. Montelibretti, DiaTHEMA Lab, Monterotondo 00015, Italy*

Biagio Pede − *Dipartimento di Scienze e Tecnologie Chimiche, Università di Roma "Tor Vergata" and Consorzio INSTM RU "Roma Tor Vergata", Rome 00133, Italy; Istituto di Struttura della Materia (ISM), Consiglio Nazionale delle Ricerche (CNR), Sez. Montelibretti, DiaTHEMA Lab, Monterotondo 00015, Italy*

Matteo Mastellone − *Istituto di Struttura della Materia (ISM), Consiglio Nazionale delle Ricerche (CNR), Sez. Montelibretti, DiaTHEMA Lab, Monterotondo 00015, Italy*

Valerio Serpente − *Istituto di Struttura della Materia (ISM), Consiglio Nazionale delle Ricerche (CNR), Sez. Montelibretti, DiaTHEMA Lab, Monterotondo 00015, Italy*

Veronica Valentini − *Istituto di Struttura della Materia (ISM), Consiglio Nazionale delle Ricerche (CNR), Sez. Montelibretti, DiaTHEMA Lab, Monterotondo 00015, Italy*

Alessandro Bellucci − *Istituto di Struttura della Materia (ISM), Consiglio Nazionale delle Ricerche (CNR), Sez. Montelibretti, DiaTHEMA Lab, Monterotondo 00015, Italy*

Daniele M. Trucchi − *Istituto di Struttura della Materia (ISM), Consiglio Nazionale delle Ricerche (CNR), Sez. Montelibretti, DiaTHEMA Lab, Monterotondo 00015, Italy*

Fabio Domenici − *Dipartimento di Scienze e Tecnologie Chimiche, Università di Roma "Tor Vergata" and Consorzio INSTM RU "Roma Tor Vergata", Rome 00133, Italy*; orcid.org/0000-0001-6776-2737

Complete contact information is available at: https://pubs.acs.org/10.1021/acsomega.3c03080

Notes

The authors declare no competing financial interest.

ACKNOWLEDGMENTS

The authors acknowledge INSTM (the National Interuniversity Consortium of Materials Science and Technology) project INSTM23POLINI "Sviluppo di celle solari ad alte temperature basate su emettitori foto-termoionici," and the TECHPRO "Thermionic Energy Conversion for High Power RadiatiOn" project no. 2022KXKR3S funded by the Italian Ministry of University and Research within the framework of the EU Programme Next Generation Europe.

ADDITIONAL NOTES

[1]Several Authors in the relevant literature refer to seeds as nuclei; consequently, the terms "seeding density" and "nucleation density" are used as synonyms. We prefer to call "nuclei" those crystals that form because of a nucleation process. Diamond seeds deposited at the substrate surface after a sonication process, as well as diamond fragments that scratching pretreatments could implant in the substrate surface, should be considered as "growth centers", not as "nuclei", in that they do not originate at the solid−gas interface via a heterogeneous nucleation process during CVD.

[2]Details on the surface chemistry of DND in suspension are given in ref 22.

[3]We do not consider intentionally the amorphous sp^2 carbon shell that surrounds DND particles in that (i) it is supposed to be quickly etched away in the presence of atomic hydrogen in the CVD reactor and (ii) its thickness, estimated from either NMR spectroscopy or HR-TEM images, is the 0.4−0.6 nm interval.[43,44] These facts could modify the effective size of sp^3 seeds by few tenths of nm, i.e., a quantity well below the resolution of the experimental techniques we have used (DLS, FEG SEM).

[4]We have used $\sigma = 3.6\ J/m^2$, hence $c = \frac{2\sigma v_m}{RT} = \frac{2 \times 3.6 \times 3.439 \times 10^{-6}}{8.31 \times 973}$ $= 3.06 \times 10^{-9}$ $m = 3.06$ nm.

[5]A hemispherical diamond nucleus with radius 0.7 nm contains 120−130 carbon atoms.

REFERENCES

(1) Field, J. E. *The Properties of Diamond*; Academic Press: London, 1979.

(2) Handschuh-Wang, S.; Wang, T.; Tang, Y. Ultrathin Diamond Nanofilms − Development, Challenges, and Applications. *Small* **2021**, *17*, No. 2007529.

(3) Zhu, W.; Kochanskj, P.; Jin, S. Low-Field Electron Emission from Undoped Nanostructured Diamond. *Science* **1998**, *282*, 1471−1473.

(4) Lions, M.; Saada, S.; Bazin, B.; Pinault, M.-A.; Jomard, F.; Andrieu, F.; Faynot, O.; Bergonzo, P. Extreme insulating ultrathin diamond films for SOD applications: From coalescence modelling to synthesis. *Diamond Relat. Mater.* **2010**, *19*, 413−417.

(5) Zalieckas, J.; Mondragon, I. R.; Pobedinskas, P.; Kristoffersen, A. S.; Mohamed-Ahmed, S.; Gjerde, C.; Høl, P. J.; Hallan, G.; Furnes, O. N.; Cimpan, M. R.; Haenen, K.; Holst, B.; Greve, M. M. Polycrystalline diamond coating on orthopedic implants: realization and role of surface topology and chemistry in adsorption of proteins and cell proliferation. *ACS Appl. Mater. Interfaces* **2022**, *14*, 44933−44946.

(6) Bellucci, A.; Pede, B.; Mastellone, M.; Valentini, V.; Polini, R.; Trucchi, D. M. Thermionic performance of nanocrystalline diamond/silicon structures under concentrated solar radiation. *Ceram. Int.* **2023**, *49*, 24351−24355.

(7) Wrachtrup, J.; Jelezko, F. Processing quantum information in diamond. *J. Phys. Condens. Matter* **2006**, *18*, S807−S824.

(8) Mochalin, V. N.; Shenderova, O.; Ho, D.; Gogotsi, Y. The properties and applications of nanodiamonds. *Nat. Nanotechnol.* **2012**, *7*, 11−23.

(9) Liu, H., Dandy, D. S. *Diamond Chemical Vapour Deposition: Nucleation and Early Growth Stages*; Bunshah, R. F., McGuire, G. E., Rossnagel, S. M. Noyes: Park Ridge, NJ, 1995; Chapter 7, pp. 150−159.

(10) Polini, R.; Tomellini, M.; Fanfoni, M.; le Normand, F. Dirac δ nucleation in the framework of Avrami's model: the case of diamond growth on deformed Si(100). *Surf. Sci.* **1997**, *373*, 230−236.

(11) (a) Girard, H. A.; Perruchas, S.; Gesset, C.; Chaigneau, M.; Vieille, L.; Arnault, J.-C.; Bergonzo, P.; Boilot, J.-P.; Gacoin, T.

Electrostatic Grafting of Diamond Nanoparticles: A Versatile Route to Nanocrystalline Diamond Thin Films. *ACS Appl. Mater. Interfaces* **2009**, *1*, 2738−2746. (b) Arnault, J. C., Girard, H. A. Diamond Nucleation and Seeding Techniques: Two Complementary Strategies for the Growth of Ultra-thin Diamond Films. In *Nanodiamond*; The Royal Society of Chemistry, 2014; pp. 221−252, and references therein.

(12) Janssens, S. D.; Vázquez-Cortés, D.; Fried, E. Formation and morphology of closed and porous films grown from grains seeded on substrates: Two-dimensional simulations. *Acta Mater.* **2022**, *225*, No. 117555.

(13) Tomellini, M.; Polini, R. Impact of seed density on continuous ultrathin nanodiamond film formation. *Diamond Relat. Mater.* **2023**, *133*, No. 109700.

(14) Liu, H.; Dandy, D. S. Studies on nucleation process in diamond CVD: an overview of recent developments. *Diamond Relat. Mater.* **1995**, *4*, 1173−1188.

(15) Arnault, J. C.; Intiso, L.; Saada, S.; Delclos, S.; Bergonzo, P.; Polini, R. Effect of 3C-SiC(100) initial surface stoichiometry on bias enhanced diamond nucleation. *Appl. Phys. Lett.* **2007**, *90*, No. 044101.

(16) Anupam, K. C.; Saha, R.; Anderson, J.; Ayala, A.; Engdahl, C.; Piner, E. L.; Holtz, M. W. Effect of seeding density on the growth of diamond films by hot-filament chemical vapor deposition from sparse to dense range. *J. Appl. Phys.* **2021**, *130*, 225302.

(17) Stehlik, S.; Varga, M.; Ledinsky, M.; Miliaieva, D.; Kozak, H.; Skakalova, V.; Mangler, C.; Pennycook, T. J.; Meyer, J. C.; Kromka, A.; Rezek, B. High-yield fabrication and properties of 1.4 nm nanodiamonds with narrow size distribution. *Sci. Rep.* **2016**, *6*, 38419.

(18) Stehlik, S.; Varga, M.; Stenclova, P.; Ondic, L.; Ledinsky, M.; Pangrac, J.; Vanek, O.; Lipov, J.; Kromka, A.; Rezek, B. Ultrathin Nanocrystalline Diamond Films with Silicon Vacancy Color Centers via Seeding by 2 nm Detonation Nanodiamonds. *ACS Appl. Mater. Interfaces* **2017**, *9*, 38842−38853.

(19) Ivanov, O. A.; Muchnikov, A. B.; Chernov, V. V.; Bogdanov, S. A.; Vikharev, A. L.; Butler, J. E. Experimental study of hydrogen plasma etching of (100) single crystal diamond in a MPACVD reactor. *Mater. Lett.* **2015**, *151*, 115−118.

(20) Yurov, V.; Bushuev, E.; Bolshakov, A.; Ashkinazi, E.; Antonova, I.; Zavedeev, E.; Khomich, A.; Voronov, V.; Ralchenko, V. Etching Kinetics of (100) Single Crystal Diamond Surfaces in a Hydrogen Microwave Plasma, Studied with In Situ Low-Coherence Interferometry. *Phys. Status Solidi A* **2017**, *214*, No. 1700177.

(21) Thomas, E. L. H.; Mandal, S.; Ahmed, A.-I.; Macdonald, J. E.; Dane, T. G.; Rawle, J.; Cheng, C.-L.; Williams, O. A. Spectroscopic Ellipsometry of Nanocrystalline Diamond Film Growth. *ACS Omega* **2017**, *2*, 6715−6727.

(22) Shenderova, O.; Hens, S.; McGuire, G. Seeding slurries based on detonation nanodiamond in DMSO. *Diamond Relat. Mater.* **2010**, *19*, 260−267.

(23) Arnault, J. C.; Saada, S.; Williams, O. A.; Haenen, K.; Bergonzo, P.; Nesladek, M.; Polini, R.; Osawa, E. Surface characterization of silicon substrates seeded with diamond nanoparticles under UHV annealing. *Phys. Stat. Sol. (a)* **2008**, *205*, 2108−2113.

(24) Arnault, J. C.; Saada, S.; Nesladek, M.; Williams, O. A.; Haenen, K.; Bergonzo, P.; Osawa, E. Diamond nanoseeding on silicon: Stability under H_2 MPCVD exposures and early stages of growth. *Diamond Relat. Mater.* **2008**, *17*, 1143−1149.

(25) Arnault, J. C.; Hubert, S.; Le Normand, F. Silicon Etching during the HFCVD Diamond Growth. *J. Phys. Chem. B* **1998**, *102*, 4856−4864.

(26) Giussani, A.; Janssens, S. D.; Vázquez-Cortés, D.; Fried, E. Evolution of nanodiamond seeds during the chemical vapor deposition of diamond on silicon substrates in oxygen-rich plasmas. *Appl. Surf. Sci.* **2022**, *581*, No. 152103.

(27) Battaile, C. C.; Srolovitz, D. J.; Oleinik, I. I.; Pettifor, D. G.; Sutton, A. P.; Harris, S. J.; Butler, J. E. Etching effects during the chemical vapor deposition of (100) diamond. *J. Chem. Phys.* **1999**, *111*, 4291−4299.

(28) Barnard, A. S. Modeling polydispersive ensembles of diamond nanoparticles. *Nanotechnology* **2013**, *24*, No. 085703.

(29) Wang, C. X.; Yang, G. W. Thermodynamics of metastable phase nucleation at the nanoscale. *Mater. Sci. Eng. R.* **2005**, *49*, 157−202.

(30) Jiang, Q.; Li, J. C.; Wilde, G. The size dependence of the diamond-graphite transition. *J. Phys.: Condens. Matter* **2000**, *12*, 5623−5627.

(31) Molinari, E.; Polini, R.; Sessa, V.; Terranova, M. L.; Tomellini, M. Diamond nucleation from the gas phase: A kinetic approach. *J. Mater. Res.* **1993**, *8*, 785−797.

(32) Haase, R. *Thermodynamics of irreversible processes*; Dover Publications, Inc.: New York, 1990, Chapter 2.

(33) Gurman, E. M. *Mechanochemistry of Solid Surfaces*; World Scientific Publishing Co. Pte. Ltd.: Singapore, 1994.

(34) Halicioglu, T. Calculation of surface energies for low index planes of diamond. *Surf. Sci. Lett.* **1991**, *259*, L714−L718.

(35) Frenklach, M.; Wang, H. Detailed surface and gas-phase chemical kinetics of diamond deposition. *Phys. Rev. B* **1991**, *43*, 1520−1545.

(36) Mutaftschiev, B. *The atomistic nature of crystal growth*; Springer-Verlag: Berlin, 2001.

(37) Mahon, P.; Pailthorpe, B. A.; Bacskay, G. B. A quantum mechanical calculation of interatomic interactions in diamond. *Philos. Mag. B* **1991**, *63*, 1419−1430. and references therein

(38) Davis, R. F. Silicon Carbide In *Reference Module in Materials Science and Materials Engineering*; Elsevier, 2017; pp. 1−6.

(39) Wang, J.; Huang, X.; Zhang, H.; Wang, L.; Huang, W.; Kuang, S.; Huang, F. Diamond (001)−Si(001) and Si(001)−Ti(0001) interfaces: A density functional theory study. *J. Phys. Chem. Solids* **2021**, *150*, No. 109865.

(40) Lee, S. T.; Peng, H. Y.; Zhou, X. T.; Wang, N.; Lee, C. S.; Bello, I.; Lifshitz, Y. A nucleation site and mechanism leading to epitaxial growth of diamond films. *Science* **2000**, *287*, 104−106.

(41) Lifshitz, Y.; Köhler, T.; Frauenheim, T.; Guzmann, I.; Hoffman, A.; Zhang, R. Q.; Zhou, X. T.; Lee, S. T. The Mechanism of Diamond Nucleation from Energetic Species. *Science* **2002**, *297*, 1531−1533.

(42) Gebbie, M. A.; Ishiwata, H.; McQuade, P. J.; Petrak, V.; Taylor, A.; Freiwald, C.; Dahl, J. E.; Carlson, R. M. K.; Fokin, A. A.; Schreiner, P. R.; Shen, Z.-X.; Nesladek, M.; Melosh, N. A. Experimental measurement of the diamond nucleation landscape reveals classical and nonclassical features. *Proc. Natl. Acad. Sci. U. S. A.* **2018**, *115*, 8284−8289.

(43) Ducrozet, F.; Girard, H.; Leroy, J.; Larquet, E.; Florea, I.; Brun, E.; Sicard-Roselli, C.; Arnault, J.-C. New insights into the reactivity of detonation nanodiamonds during the first stages of graphitization. *Nanomaterials* **2021**, *11*, 2671.

(44) Fang, X.; Mao, J.; Levin, E. M.; Schmidt-Rohr, K. Nonaromatic Core-Shell Structure of Nanodiamond from Solid-State NMR Spectroscopy. *J. Am. Chem. Soc.* **2009**, *131*, 1426−1435.

https://doi.org/10.1021/acsomega.3c03080
ACS Omega 2023, 8, 25496−25505